Imperfect traveling chimera states induced by local synaptic gradient coupling

Bidesh K. Bera,[1,*] Dibakar Ghosh,[1,†] and Tanmoy Banerjee[2,‡]

[1]*Physics and Applied Mathematics Unit, Indian Statistical Institute, Kolkata-700 108, India*

[2]*Chaos and Complex Systems Research Laboratory, Department of Physics, University of Burdwan, Burdwan 713 104, West Bengal, India*

(Received 26 April 2016; revised manuscript received 23 June 2016; published 14 July 2016)

In this paper, we report the occurrence of chimera patterns in a network of neuronal oscillators, which are coupled through *local*, synaptic *gradient* coupling. We discover a new chimera pattern, namely the *imperfect traveling chimera state*, where the incoherent traveling domain spreads into the coherent domain of the network. Remarkably, we also find that chimera states arise even for *one-way* local coupling, which is in contrast to the earlier belief that only nonlocal, global, or nearest-neighbor local coupling can give rise to chimera state; this find further relaxes the essential connectivity requirement of getting a chimera state. We choose a network of identical bursting Hindmarsh-Rose neuronal oscillators, and we show that depending upon the relative strength of the synaptic and gradient coupling, several chimera patterns emerge. We map all the spatiotemporal behaviors in parameter space and identify the transitions among several chimera patterns, an in-phase synchronized state, and a global amplitude death state.

DOI: 10.1103/PhysRevE.94.012215

I. INTRODUCTION

Research on the collective behavior of *identical* oscillators has been revitalized with the discovery of the chimera state [1]. Kuramoto and Battogtokh [2] discovered that the population of identical oscillators is subdivided into two incongruous domains: in one domain the neighboring oscillators are synchronized, whereas in another domain the oscillators are desynchronized. This intriguing spatiotemporal state was named the chimera state by Strogatz [3], and it has been in the center of attention over the past decade. Since its discovery in phase oscillators under nonlocal coupling by Kuramoto and Battogtokh [2], other chimera states have also been discovered. An amplitude-mediated chimera state was reported in [4], where, under strong *global coupling*, a network of complex Ginzberg-Landau oscillators show fluctuations in both the phase and amplitude part in the incoherent region. Later, an *amplitude chimera* state was discovered by Zakharova *et al.* [5] where all the oscillators in a network have the same phase velocity but differ in amplitude in the incoherent region. Recently, a chimera state was observed also in *local* nearest-neighbor coupling [6–8], which proves that nonlocal or strong global coupling is not an essential requirement to achieve a chimera state.

The robustness of the chimera state has been proved through a series of experiments: The first experimental observation of a chimera state was reported in an optical system [9] and chemical oscillators [10]. Later, a chimera state was observed experimentally in several other systems, e.g., in a mechanical system [11] and a time-delay laser system [12], to name a few. Recently, Hart *et al.* [13] reported the experimental observation of a chimera state in a globally coupled minimal network of four optoelectronic oscillators. Apart from these manmade experimental setups, the occurrence of a chimera state has been reported in real physical and biological systems, e.g., in SQUID metamaterial [14,15], ecology [16,17], and quantum systems [18].

Ever since its discovery, the chimera state has been strongly connected to several neuronal processes, such as the unihemispheric slow-wave sleep of some aquatic mammals, such as dolphins, eared seals, and manatees [19,20], and some migratory birds [20]. During slow-wave sleep, these species shut down only one cerebral hemisphere of the brain and close the opposite eye. During this time, the other half of the brain monitors what is going on in the environment (for migratory birds) and controls breathing functions (for aquatic mammals). This strongly indicates that in the awake part of the cerebral hemisphere, neuronal oscillators are desynchronized, while in the sleepy part neuronal oscillators are very much synchronized, which resembles the chimera state. Recently, Hizanidis *et al.* [21] established the occurrence of a chimera state in a neural network based on the *C. elegans* soil worm connectome in terms of Hindmarsh-Rose dynamics.

Therefore, systematic studies on the chimera state in neuronal systems deserve special attention. Earlier works on a network of neuronal oscillators considered the FitzHugh-Nagumo model with type-II excitability [22,23] and the SNIPER model of type-I excitability [24]; those works dealt with spiking neurons (as those models could not produce bursting behavior). In this context, neuronal oscillation modeled by the Hindmarsh-Rose (HR) model is much more realistic because, depending upon parameter values, it shows both type-I and type-II excitability and can produce a plethora of physiologically relevant neuronal oscillations, such as square wave bursting (both periodic and chaotic), plateau bursting, spiking, mixed mode bursting, etc. Hizanidis *et al.* [25] reported the occurrence of a chimera state in a network of HR neurons under nonlocal coupling. However, the considered nonlocal coupling has an ideal rectangular kernel, which has less biological relevance as far as the coupling function is concerned.

In this context, synaptic coupling is one of the most realistic coupling schemes through which neurons are connected. In the context of interneuronal communication, two variants of synapses exist, namely chemical and electrical synapses.

*bideshbera18@gmail.com

†diba.ghosh@gmail.com

‡tbanerjee@phys.buruniv.ac.in

Bera *et al.* [8] considered the chemical synaptic coupling with nonlocal, global, and local nearest-neighbor coupling topology, and they established the occurrence of a chimera state. In that work, however, only excitatory coupling with symmetric synaptic coupling strength was considered in all three coupling topologies. Normally, in a network of neuronal oscillators, both excitatory and inhibitory interactions are present [26]. In the absence of time delay, in general, fast excitatory coupling leads to synchronization and fast inhibitory coupling promotes antisynchronization. Belykh *et al.* [27] showed that the synergistic effect of excitation and inhibition leads to complete synchronization (i.e., synchrony in both burst and spike) with a lower coupling threshold. Thus, it is important to study their simultaneous effect on the occurrence of multicluster synchrony or a chimera state. The simultaneous effect of excitatory and inhibitory coupling is best represented by *gradient coupling*: in this coupling scheme, one can control the strength of excitation and inhibition by simply controlling the parameter associated with gradient coupling. Earlier, the effect of gradient coupling was studied in the context of oscillation suppression in nonlinear oscillators with time-delay diffusive coupling [28], synchronization of nonlinear coupled systems [29], and control of spatiotemporal chaotic systems [30,31], but its influence on the occurrence of a chimera state has not been studied yet.

In this paper, we investigate the effect of local chemical *synaptic gradient* coupling on the occurrence of a chimera state. We choose a network of identical square-wave bursting Hindmarsh-Rose neuronal oscillators, and we show that depending upon the proper choice of the coupling parameter associated with the gradient coupling, we can attain three different coupling topologies, namely *one-way* excitatory local coupling, nearest-neighbor *asymmetric* excitatory coupling, and *simultaneous excitatory-inhibitory* coupling. Remarkably, we find a chimera state even in the *one-way* excitatory local coupling that further relaxes the essential requirement of getting a chimera state in a network. We identify and confirm the occurrence of a new chimera pattern, namely the *imperfect traveling chimera* state in the network with nearest-neighbor asymmetric excitatory coupling. We further map in parameter space the transitions among chimera patterns, synchronized states, and the amplitude death state with the variation of the synaptic and gradient coupling strengths.

II. COUPLING SCHEME

We consider a network of N identical Hindmarsh-Rose neurons [32,33] coupled via a local synaptic *gradient* coupling given by

$$\dot{x_i} = ax_i^2 - x_i^3 - y_i - z_i + (V_s - x_i)[(\epsilon + r)\Gamma(x_{i+1}) + (\epsilon - r)\Gamma(x_{i-1})], \tag{1a}$$

$$\dot{y_i} = (a + \alpha)x_i^2 - y_i, \tag{1b}$$

$$\dot{z_i} = \mu(bx_i + c - z_i), \tag{1c}$$

$i = 1,2,\ldots,N$ ($N \geqslant 3$). The variable x_i represents the membrane potential of the ith HR neuron, y_i is the fast current (associated with Na^+ or K^+), and z_i represents the slow current (associated with Ca^{2+}). The parameter μ determines the ratio of slow-fast time scales. The sigmoidal function $\Gamma(x_i) = 1/\{1 + \exp[-\lambda(x_i - \Theta_s)]\}$ represents the fast threshold modulation synaptic coupling [34], where λ determines the slope of the function and Θ_s is the firing threshold. We use the periodic boundary condition ($x_{N+1} = x_1$). We take the reversal potential $V_s = 2$ such that $V_s > x_i(t)$ is always satisfied; also, we choose the synaptic threshold $\Theta_s = -0.25$ to ensure that every spike in a burst can reach the threshold value [27,34] and the slope of the sigmoidal function $\lambda = 10$.

The most interesting and important part of the coupling function of (1) is the gradient coupling: if we choose $r = 0$, then Eq. (1) represents a synaptic nearest-neighbor *excitatory* coupling with the synaptic coupling strength $\epsilon(> 0)$. But, for $r > 0$, depending upon the relative values of r and ϵ, three different scenarios can be implemented:

Case I $\epsilon > r$: Here we have excitatory coupling [since $(\epsilon \pm r) > 0$], but now the ith neuron is coupled to its nearest neighbors with two different synaptic coupling strengths; this introduces *asymmetry* in the coupling.

Case II $\epsilon = r$: This condition represents one-way local excitatory coupling with the effective synaptic coupling strength 2ϵ. As $V_s > x_i(t)$ for all time t and $x_i(t)$, the coupling is positive and the synapse is excitatory, i.e., the input from the $(i + 1)$th neuron to the ith neuron can enhance the activity of this neuron.

Case III $\epsilon < r$: Now the ith neuron is connected to the $(i + 1)$th neuron through an *excitatory* coupling with an effective synaptic coupling strength $(\epsilon + r)$, but it is connected to the $(i - 1)$th neuron via an *inhibitory* coupling with an effective synaptic coupling strength $(\epsilon - r)$. In this case, the input to the ith neuron from the $(i + 1)$th neuron via synaptic coupling can enhance its activity, and that from the $(i - 1)$th neuron via synaptic coupling can suppress its activity. Thus, this condition leads to the simultaneous occurrence of excitation and inhibition in the HR-neuron network, which is the most important case in the context of neuroscience. Therefore, we denote r (> 0), which governs the strength as well as the nature of the coupling, as the *gradient coupling strength*, and ϵ (> 0) as the *synaptic* coupling strength.

In the following, we will explore the dynamics of the network under these three distinct coupling conditions; our main emphasis will be to identify the parameter region of the synaptic and gradient coupling strengths where the chimera state occurs.

III. RESULTS

We explore the spatiotemporal dynamics of the considered network under three different relative values of ϵ and r. We consider $N = 200$ and integrate Eq. (1) using the fourth-order Runge-Kutta algorithm (step size $= 0.001$). In all the simulations, we use an asymmetric V-shaped profile for initial conditions: The following initial conditions are used: $x_m = 0.05(99 - m)$, $x_n = 0.012(n - 100)$, $y_m = 0.01(99 - m)$, $y_n = 0.02(n - 100)$, $z_m = 0.0151(99 - m)$, and $z_n = 0.0201(n - 100)$ (where $m = 1,\ldots,100$ and $n = 101,\ldots,200$). We have also checked for the random initial conditions uniformly distributed in the range $(-2,2)$ and find *qualitatively* the same chimera patterns. Thus, we understand that, in the present case, the important factor is

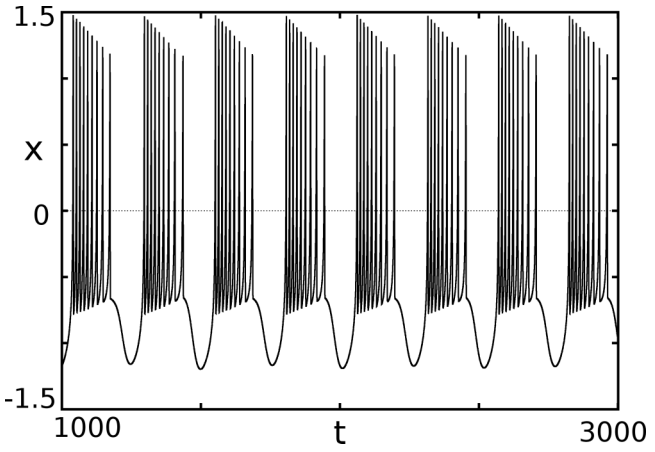

FIG. 1. Square wave bursting: time series of x of an individual HR neuron given by Eq. (1) ($a = 2.8$, $\alpha = 1.6$, $c = 5$, $b = 9$, and $\mu = 0.001$).

the inhomogeneous starting points for each oscillator in phase space. Also, we examine the lifetime of the observed chimera states for a sufficiently long time and ensure that it is not a transient chimera like the amplitude chimera state. Throughout the paper, we use the following system parameters of HR neurons: $a = 2.8$, $\alpha = 1.6$, $c = 5$, $b = 9$, and $\mu = 0.001$. With these system parameters, an isolated HR neuron exhibits square-wave bursting (see Fig. 1).

A. Case I: $\epsilon > r$, asymmetric excitatory coupling: Imperfect traveling chimera state

We start with the condition $\epsilon > r$. In this condition, the ith node is connected to the $(i+1)$th node with an effective synaptic coupling strength $(\epsilon + r)$, whereas it is connected to the $(i-1)$th node with an effective synaptic coupling strength $(\epsilon - r)$. Since $\epsilon > r$, the coupling is always excitatory in nature with asymmetric coupling strengths.

We fix the value of the gradient coupling strength at $r = 0.2$ and vary the synaptic coupling strength ϵ. For lower values of ϵ ($\epsilon \lesssim 0.5$), all of the neurons exhibit a disordered turbulent state. With increasing ϵ we observe that the coupled system enters into a state where certain neurons are synchronized but the remaining neurons are in an incoherent state, which is a signature of a chimera state. However, this chimera state is not static in the sense that it travels with time in the spatiotemporal domain. Significantly, this state is not a pure traveling chimera state, as during its travel some synchronized neurons are added to the traveling incoherent state. This type of traveling chimera state where the incoherent domain spreads to the synchronized domain is a *new observation*, and we call it an *imperfect traveling chimera state*. Earlier, Refs. [35,36] reported the existence of an imperfect chimera state in coupled oscillators and phase oscillators with inertia, but the *imperfect traveling chimera state* has not been reported previously. The scenario is shown in Fig. 2: here we take an exemplary value $\epsilon = 0.7$ and $r = 0.2$ (note that $\epsilon > r$). Figure 2(a) shows the time evolution of the membrane potential of all neurons for a long time run. This spatiotemporal plot clearly shows that the spatiotemporal patterns of varying width are traveling in space

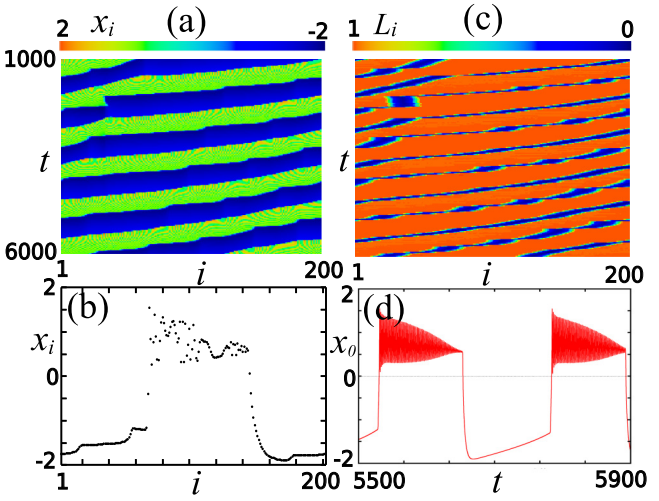

FIG. 2. $\epsilon > r$: Imperfect traveling chimera state of an ensemble of HR-neurons with asymmetric excitatory local coupling. (a) Spatiotemporal plot as a function of the neuron index $i = 1,2,\ldots,N = 200$ for $r = 0.2$ and $\epsilon = 0.7$ ($\epsilon > r$). (b) Snapshot of the variable x_i at $t = 2000$, (c) local order parameter with node index i. Red (gray) indicates coherent and blue (dark gray) represents incoherent domains. (d) Time series of an individual neuron x_0.

and time. Figure 2(b) shows a snapshot of all the neurons at time $t = 2000$. The spatial coexistence of coherent and incoherent neurons can be clearly observed from the snapshot.

To characterize the coherence-incoherence pattern and chimera state, we use the notion of *local order parameter* (note that since here we have a traveling chimera state, the mean phase velocity is not an appropriate measure). The local order parameter actually represents the local ordering of the oscillators and thus the degree of (in)coherency; it is defined as [17,37]

$$L_i = \left| \frac{1}{2\delta} \sum_{|i-k| \leqslant \delta} e^{j\Phi_k} \right|, \tag{2}$$

where $j = \sqrt{-1}, i = 1,2,\ldots,N$ and δ is the nearest neighbors on both sides of the ith oscillator. Here, we define $\Phi_i = \arctan(y_i/x_i)$ as the geometric phase of the ith HR neuron, which is a good approximation as long as μ is small ($\ll 1$). The local order parameter of the ith neuron, $L_i \approx 1$, indicates that the ith neuron belongs to the coherent part of the chimera state, i.e., $L_i = 1$ means maximum ordering or coherency. On the other hand, $L_i \approx 0$ represents that the ith neuron belongs to the incoherent neighboring nodes. We take the window size of spatial average as $\delta = 12$ and compute the local order parameter L_i of each neuron for a long time interval, which is shown in Fig. 2(c). The red (gray) region represents the coherent nodes, and in between two consecutive traveling coherent domains we have incoherent traveling domains [represented in blue (dark gray)]. It is important to note that the width of the incoherent blue (dark gray) domain changes as it travels in space: this indicates the spreading of the incoherent domain to the synchronized domain, which is a clear signature of the *imperfect traveling chimera state*. The local dynamics, i.e., the dynamics of each neuron in this chimera state, are

identical, and a typical time series of a single HR neuron is shown in Fig. 2(d), which shows that individual neurons are in *plateau bursting* mode. We also examine the effect of network size on the occurrence of an imperfect traveling chimera, and we find that it remains qualitatively unchanged even for a smaller network size (see Appendix). For coupled oscillators under *nonlocal coupling*, it has been shown in Ref. [38] that a smaller network size gives rise to distortion and a finite lifetime of a chimera state. In our case, however, the qualitative similarity of the traveling chimera state in both large as well as small networks may be attributed to the *local* nature of the coupling, where an oscillator only experiences the effect of the nearest neighbors and does not react to all the other oscillators present in the system. However, this heuristic argument needs quantitative support by investigating how network size affects the chimera pattern in *local coupling*.

For a very narrow region in parameter space, we observe that the "imperfectness" of the imperfect traveling chimera state increases for slightly lower values of ϵ in comparison with the ϵ value for which the imperfect traveling chimera state occurs. Figure 3 shows this case for $\epsilon = 0.56$ ($r = 0.2$). Here we can observe that the chimera state travels erratically in space and time; also, a new domain is created (destroyed) from (to) a completely different type of domain [see Fig. 3(a)]. This is also clearly seen in Figs. 3(b) and 3(c): here Fig. 3(b) shows the snapshot at $t = 1750$ that shows a one-headed chimera state, but at $t = 2250$ a two-headed chimera state is created, which is shown in Fig. 3(c). Interestingly, the behavior of the individual neurons at this state shows a mixed mode oscillation of square-wave bursting and plateau bursting, which is shown in Fig. 3(d).

Apart from chimera patterns, we also investigate the collective behavior of the network at larger values of ϵ. For increasing ϵ (fixed r), beyond the imperfect traveling chimera

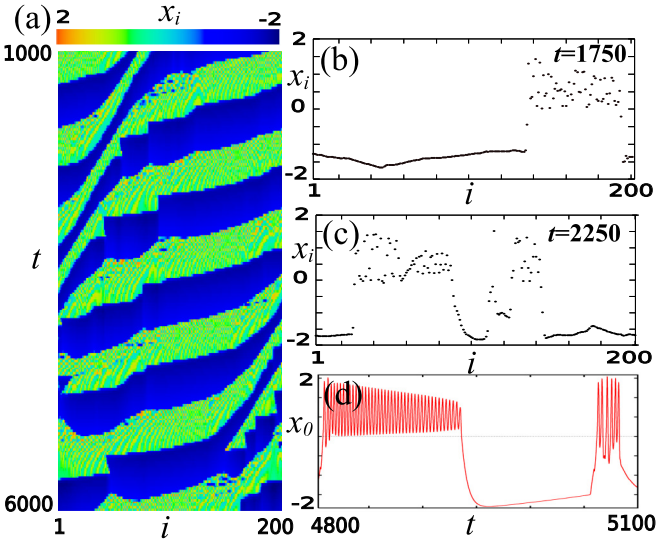

FIG. 3. $r = 0.2$ and $\epsilon = 0.56$ ($\epsilon > r$): Imperfect traveling chimera state with increasing imperfection. (a) Spatiotemporal plot as a function of the neuron index $i = 1,2,\ldots,N = 200$. Snapshot of the variable x_i at (b) $t = 1750$ showing *one-headed chimera* state, (c) $t = 2250$ showing *two-headed chimera* state. (d) Time series of an individual neuron x_0.

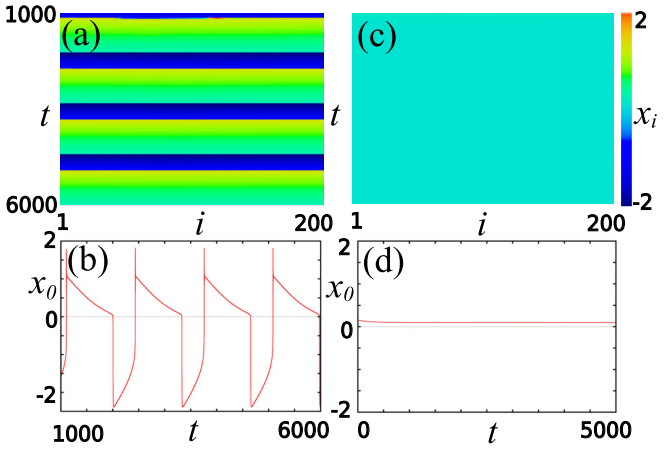

FIG. 4. $\epsilon > r$, $r = 0.2$: (a) $\epsilon = 1.3$, globally synchronized populations of neurons. (b) The corresponding time series of a single neuron. (c) $\epsilon = 1.6$, global amplitude death. (d) The corresponding time series of a single neuron.

state the network shows global synchrony. This is shown in Fig. 4(a) for $\epsilon = 1.3$. Note that here individual neurons show plateau bursting [Fig. 4(b)]. Further increase in ϵ results in global amplitude death [Fig. 4(c)] where the oscillations of all the neurons cease. Figure 4(d) shows the time series of an individual neurons. The transition from oscillatory state to amplitude death state has a broad relevance in neuroscience where we can control the neuronal outputs using this local chemical synaptic coupling.

At this point it is interesting to note the change in the time series with increasing ϵ. For the asynchronous state the HR neurons exhibit square-wave bursting (not shown), but with increasing ϵ the square-wave bursting changes into plateau bursting [Fig. 2(d)] (via the disappearance of homoclinic bifurcation [27]), through a mixed time series of square-wave and plateau bursting [Fig. 3(d)]. In the synchronized state, neurons show a pure plateau bursting that agrees with the observation of Belykh *et al.* [34] that plateau bursting promotes synchrony. The frequency of plateau bursting decreases with increasing ϵ, and it eventually reaches an infinite period, i.e., now global amplitude death emerges [Fig. 4(d)]: this typical pattern suggests that amplitude death appears through a saddle-node bifurcation [39].

B. Case II: $\epsilon = r$, one-way excitatory coupling: Imperfect chimera state and traveling chimera state

As we discussed earlier for $\epsilon = r$, each ith neuron is connected to the $(i+1)$th neuron with an effective synaptic coupling strength of 2ϵ. If we increase ϵ from a lower value, we observe complete turbulence up to $\epsilon \approx 0.5$. We find two chimera patterns beyond that: one is an *imperfect chimera* state that occurs for a small range of ϵ, and beyond that is the *traveling chimera* state. Figures 5(a)–5(c) show the spatiotemporal plot of the amplitude and local order parameter (L_i) and a snapshot at a time instant ($t = 3500$), respectively, for the imperfect chimera state at $\epsilon = 0.56$. The snapshot in Fig. 5(c) shows the multiheaded chimera pattern. The local order parameter [Fig. 5(b)] suggests that the incoherent region

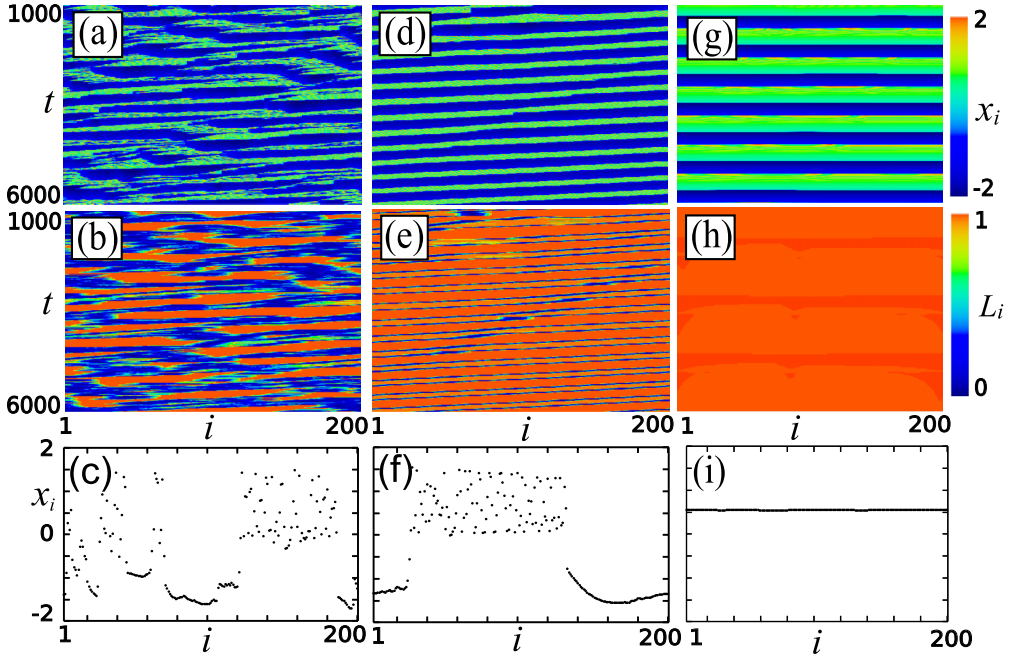

FIG. 5. One-way excitatory coupling $\epsilon = r$: (a)–(c) $\epsilon = r = 0.56$: imperfect chimera state; (a) spatiotemporal plot, (b) local order parameter, and (c) snapshot at $t = 3500$ shows multiheaded chimera state. (d)–(f) $\epsilon = r = 0.6$: traveling chimera state; (d) spatiotemporal plot, (e) local order parameter, and (f) snapshot at $t = 3500$ shows one-headed chimera state. (g)–(i) $\epsilon = r = 0.7$: synchronized state; (g) spatiotemporal plot, (h) local order parameter, and (i) snapshot at $t = 3500$ shows synchronized x_i.

[blue (dark gray)] is not static in space and time, rather it changes erratically, indicating an imperfect chimera state. Earlier, the imperfect chimera state was also observed in the Kuramoto model with inertia using nonlocal coupling [36].

The "imperfect chimera state" observed in our system [Fig. 5(a) and also see Fig. 3(a)] bears a striking resemblance to the *spatiotemporal intermittency* reported in [40] and discussed in detail in [41]. In [40], the authors considered an extension of the Oregonator oscillator, and they studied the spatiotemporal behavior under diffusive nearest-neighbor coupling: For a *fixed coupling strength*, they observed various *spatiotemporal intermittent* patterns by changing a *system parameter*. In contrast, in our present case we consider *synaptic gradient coupling*. Keeping the *system parameters fixed* (in the square-wave bursting region), we vary the *coupling strength* of the gradient coupling. Since both the HR model and the Oregonator model show slow and fast oscillations, it appears that the imperfect chimera state and the spatiotemporal intermittency share the same origin. However, any conclusive statement in this regard requires strong quantitative measures, such as the quantifiers proposed recently in Ref. [41].

If we increase the value of the synaptic coupling strength ϵ, we observe a traveling chimera state. Figures 5(d)–5(f) show the traveling chimera state at $\epsilon = 0.6$. The local order parameter [Fig. 5(e)] shows that, indeed, the incoherent (and the coherent) domain is not static in time and space. From the snapshot at $t = 3500$ [Fig. 5(f)], it is observed that the system depicts a one-headed chimera state. Further increases in ϵ result in a globally synchronized state. Figures 5(g)–5(i) depict this state for $\epsilon = 0.7$. Here the local parameter [Fig. 5(h)] attains a value $L_i \approx 1$, which indicates the presence of complete synchrony among the neurons. The snapshot at $t = 3500$ of x_i [Fig. 5(i)] supports this finding. Note that for $\epsilon = r$, synchronization occurs at a much lower value in comparison with that of $\epsilon > r$. Finally, for $\epsilon \gtrsim 1.45$, global amplitude death occurs when all the neurons come to a common steady state and achieve a quiescent state (not shown in the figure).

It is important to note that an earlier chimera state was found under nonlocal, global, and nearest-neighbor local coupling. Here, the occurrence of the chimera state even for $\epsilon = r$ actually reduces the essential requirement of the coupling function to *one-way nearest-neighbor coupling*. This finding may be extended to other coupling schemes also (i.e., other than chemical synaptic coupling). Previously, the existence of chimera states was also reported in reaction-diffusion systems, where each system is coupled locally by diffusion [6,42]. However, it should be noted that such a form of local coupling through diffusion actually has a nonlocal effect due to the fast variable. In this way, a three-component reaction-diffusion model is reduced to an effective two-component model in which the third component changes so fast that it can be eliminated adiabatically and it is represented by nonlocal coupling [43].

C. Case III: $\epsilon < r$, simultaneous excitation and inhibition: Traveling chimera state

We now explore the spatiotemporal dynamics of the considered network for $\epsilon < r$. Under this condition, a node is connected to its nearest right neighbor through an excitatory coupling, whereas it is connected to its left nearest neighbor through inhibitory coupling. Earlier, Belykh *et al.* [27] showed that the simultaneous presence of excitation and

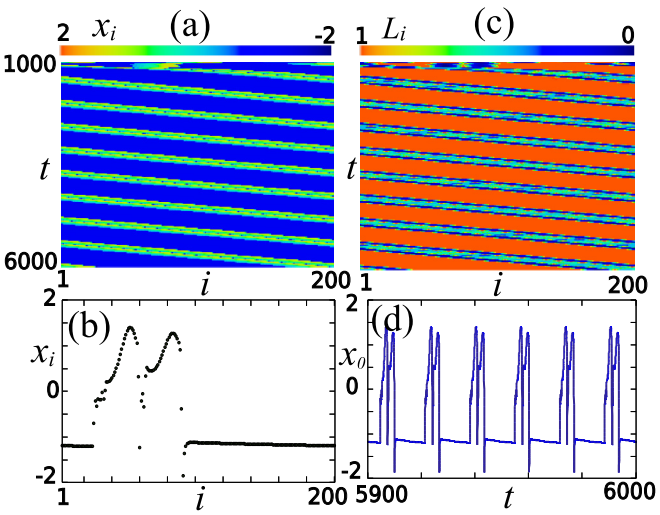

FIG. 6. $\epsilon < r$: Traveling chimera state in an ensemble of HR-neuron with excitation-inhibition local coupling $r = 8$ and $\epsilon = 0.6$. (a) Spatiotemporal plot as a function of node index $i = 1,2,\ldots,N = 200$. (b) Snapshot of the variable x_i at $t = 3300$. (c) Local order parameter with node index. Red (gray) indicates coherent domains and blue represents incoherent domains. (d) Time series of an individual neuron.

inhibition provides a synergistic effect to improve (reduce) the synchronization threshold [27]. They showed that the synchronization threshold is reduced due to the fact that the simultaneous presence of excitation and inhibition turns the dynamics from square-wave bursting to plateau bursting. Here also, we investigate the effect of the simultaneous presence of excitation and inhibition on the occurrence of a chimera state.

We choose $\epsilon = 0.6$ and increase r from 0.6 to higher values. We observe a traveling chimera state with increasing r. However, for much higher values of r, the traveling chimera state gets weaker, although the traveling wave state (not a chimera state anymore) persists. Figure 6(a) shows the spatiotemporal plot of the traveling chimera state for an exemplary value $r = 8.0$. The corresponding snapshots of x_i at $t = 3300$ are shown in Fig. 6(b). It can be observed that in the "bumplike" spatial domains, not all the nodes are incoherent; only a certain number of nodes are incoherent, whereas others maintain a phase-locked state. Note that the direction of the traveling chimera state for $\epsilon < r$ is just the *reverse* to that for $\epsilon = r$ [Fig. 5(d)] or the imperfect traveling chimera state of $\epsilon > r$ [Fig. 2(a)]. In the latter two cases, couplings are purely excitatory in nature, but for $\epsilon < r$ the coupling contains both excitatory and inhibitory connections. Thus, the change in direction of the traveling chimera state here may be attributed to the interplay of excitatory and inhibitory coupling. Figure 6(c) demonstrates the time evolution of the local order parameter L_i of all the neurons showing strips of coherent and incoherent nodes that travel with time. The red and blue regions represent the coherent and incoherent domains, respectively. It is also noteworthy to track the change in the time series with increasing r: for lower r, the individual neuron exhibits square-wave bursting, but with the increase of r, bursting changes into multiple spiking, and for large r the time series eventually shows a single spike. Figure 6(d) shows the time series corresponding to the traveling chimera state, which is a train of two pulses.

Next, we investigate whether the *inhibitory* coupling alone can give rise to a chimera state. For this we set $\epsilon = 0$ and vary r: we get an incoherent state even for higher values of r. Significantly, we find that, although excitatory coupling can induce several chimera patterns, the inhibitory coupling alone cannot induce a chimera state. However, the presence of inhibitory coupling along with excitatory coupling supports chimera and traveling chimera states. It should also be noted that for $\epsilon < 0.5$, complete turbulence occurs irrespective of the value of r; thus the chimera state and synchronization states (and also the amplitude death state) depend largely upon ϵ: only beyond a certain value of ϵ does the presence of r cause the system to show several chimera patterns.

We discussed earlier that in the case of a traveling chimera state, the mean phase velocity is not a suitable characteristic measure. An alternative way to distinguish the static and traveling chimera states is to identify the location of the neurons on a circular ring. An effective tool to identify the traveling chimera state and its traveling speed has been proposed by Hizanidis *et al.* [17]. According to their argument, in a traveling chimera state, each neuron stays part of the time in the coherent domain and part of the time in the incoherent domain without changing their spatial shape, so the maximum values of each node $x_i(t)$ will also change with time. For this purpose, we calculate the maximum values of $x_i(t)$ over a long time interval as $M(t) = \max\{x_1(t),x_2(t),\ldots,x_N(t)\}$. Similarly, one can consider the minimum values of $x_i(t)$. Figure 7(a) shows the variation of maximum values of $x_i(t)$ for a long time interval at $r = 8.0$. From this figure, the time series of $M(t)$ shows a periodic behavior, thus indicating the episodic occurrence of maxima to a certain node. The Fourier

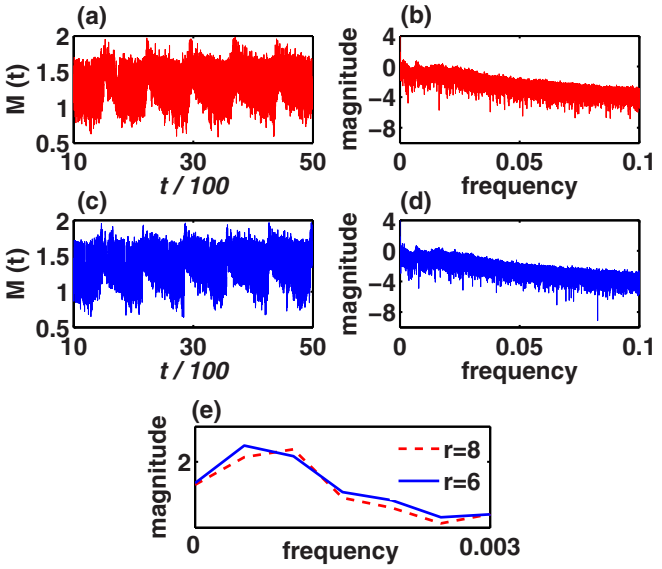

FIG. 7. Simultaneous presence of excitatory and inhibitory coupling for $\epsilon < r$: variation of maximum values of $x_i(t)$ with time t, for (a) $r = 8.0$ and (c) $r = 6.0$. The corresponding Fourier transform of $M(t)$ for (b) $r = 8.0$ and (d) $r = 6.0$. (e) Shift of maxima in the Fourier transform of $M(t)$ for $r = 8.0$ (red dashed line) and $r = 6.0$ (blue line).

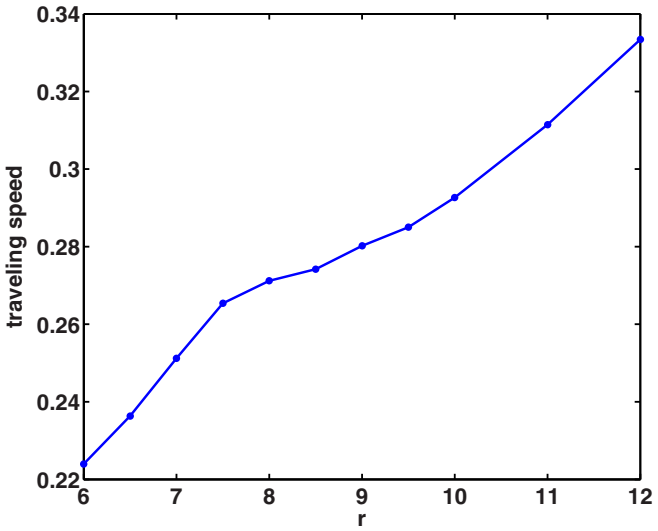

FIG. 8. Variation of traveling speed for different values of gradient coupling strength r for $\epsilon = 0.6$.

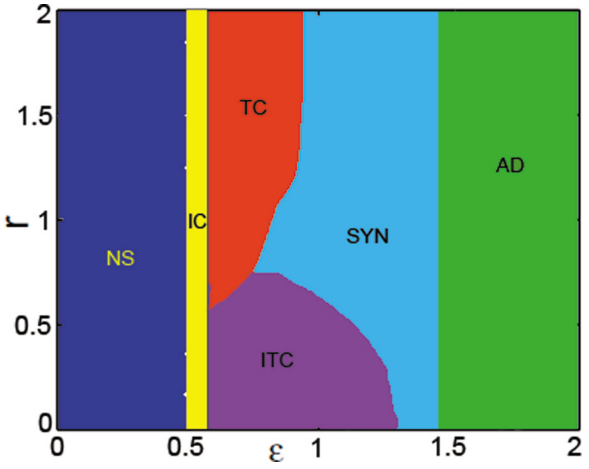

FIG. 9. Phase diagram in the ϵ-r plane. NS: turbulence or unsynchronized state, IC: imperfect chimera state, ITC: imperfect traveling chimera state, TC: traveling chimera state, SYN: global synchronized state, AD: global amplitude death.

transform of $M(t)$ determines the time period T, which is required for a single node to attain the maximum amplitude state. The Fourier transform of $M(t)$ is shown in Fig. 7(b). We find that the maximum amplitude occurs at frequency $f = 0.001\,33$ with long period $T = 1/f = 751.88$. With this time period T, the entire incoherent and coherent domains cover the whole circular ring consisting of N nodes with traveling speed $= N/T = 0.266$. At lower values of r, e.g., at $r = 6.0$, the variation of $M(t)$ is shown in Fig. 7(c) and the corresponding Fourier transform is shown in Fig. 7(d). We find that the maximum amplitude occurs at frequency $f = 0.001\,12$ with time period $T = 892.86$. At $r = 6.0$, the maximum amplitude occurs at a relatively lower frequency than that of $r = 8.0$: Fig. 7(e) shows this, where red dashed and blue solid lines correspond to $r = 8.0$ and 6.0, respectively. Figure 8 shows the variation of traveling speed for different values of r. To find the traveling speed for each r, we average over five different realizations. It can be seen that the speed of a traveling chimera state increases for increasing value of gradient coupling strength r. This is due to the fact that increasing r results in the pronounced asymmetry in the coupling [see Eq. (1a)]. Since the traveling chimera state is governed by this asymmetry, increasing r in turn increases the traveling speed.

To explore the complete spatiotemporal dynamics of the system, we compute the phase diagram in the ϵ-r parameter space (Fig. 9) for the range of $\epsilon \in [0,2]$ and $r \in [0,2]$. We change both ϵ and r with a step size of 0.01. From the phase diagram it can be noticed that the choice of ϵ and r organizes the phase diagram. Below a value of ϵ ($\epsilon \lesssim 0.5$), the network shows turbulent behavior irrespective of the value of r. Beyond that, we notice an imperfect chimera state for a very narrow region, but after this region the system shows imperfect traveling chimera for $\epsilon > r$ and a traveling chimera state for $\epsilon \leqslant r$. It can be seen from the phase diagram (Fig. 9) that for $\epsilon = r$, the system enters into global synchrony for a much lower value of ϵ. For a larger value of ϵ, all the neurons in the network eventually attain a stable homogeneous steady state and thus global amplitude death occurs in the network. In the parameter space, the separation lines of turbulence to an imperfect chimera state, imperfect chimera to a traveling chimera state, and synchronization to amplitude death are almost vertical, which means the value of synaptic coupling strength ϵ plays an important role in determining such states, while the gradient coupling strength r plays a crucial role in organizing the transition from the (imperfect) traveling chimera state to the synchronized state.

IV. CONCLUSION

In this paper, we have reported the occurrence of several chimera patterns in a network of Hindmarsh-Rose neuronal oscillators, which are connected by local chemical synaptic gradient coupling. Remarkably, we have found a chimera state even in one-way local coupling, which reduces the essential connectivity requirement to observe chimera states below nearest-neighbor local coupling. Depending on the gradient coupling parameter, we observe imperfect traveling chimera, imperfect chimera, and traveling chimera states; of these, the imperfect traveling chimera state has not been observed earlier for any other coupling scheme. We observed an imperfect traveling chimera state for asymmetric excitatory coupling, while for one-way excitatory coupling and also for simultaneous excitatory-inhibitory coupling we observed a traveling chimera state, although the direction of travel in those states is reversed. We also observed a pronounced change in the time series of the neuronal oscillators: for predominant excitation, square-wave bursting changes to plateau bursting and then amplitude death occurs; in contrast, when both inhibitory and excitatory coupling are present, with an increase in gradient coupling strength (r), square-wave bursting eventually changes into spiking behavior.

Since here we have considered nearest-neighbor and one-way local coupling, it is intuitive to observe traveling-wave solutions, but it is *counterintuitive* to observe chimera patterns. The present study is important in the context of neuroscience in the sense that this study provides evidence that local

synaptic (gradient) coupling not only provides synchrony [27] or amplitude death [39], but under certain circumstances it may drive the neuronal network to a chimera state.

ACKNOWLEDGMENTS

The authors acknowledge the anonymous referees for their insightful suggestions. T.B. acknowledges financial support from SERB, Department of Science and Technology (DST), India (Grant No. SB/FTP/PS-005/2013).

APPENDIX: IMPERFECT TRAVELING CHIMERA STATE FOR A SMALLER NETWORK

Figure 10(a) shows the imperfect traveling chimera state in a network of $N = 50$ oscillators under the same coupling scheme as Eq. (1) ($\epsilon = 0.58, r = 0.2$). Figure 10(b) shows the corresponding local order parameter L_i. Figure 10(c) shows the imperfect traveling chimera in a network of $N = 100$ oscillators for $\epsilon = 0.58$ ($r = 0.2$). Here, we use a similar asymmetric V-shaped profile for initial conditions, as discussed in Sec. III. Note the qualitative similarity among the imperfect traveling chimera states of Fig. 2 and Figs. 10(a) and 10(c). The phase diagram in the ϵ-r plane for $N = 100$ is shown in Fig. 10(d). Note that the parameter zone of getting chimera states is now reduced in comparison with that for $N = 200$ (Fig. 9). However, significantly, the qualitative structure of the whole phase diagram remains the same.

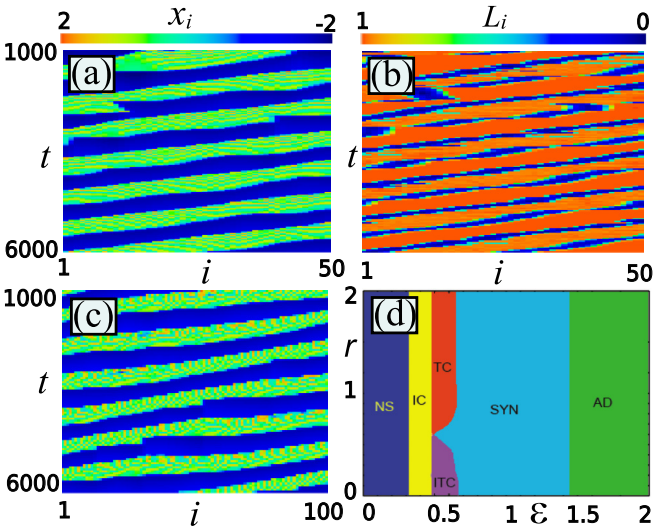

FIG. 10. $\epsilon = 0.58, r = 0.2$: (a) Imperfect traveling chimera state and (b) local order parameter L_i for $N = 50$. (c) Imperfect traveling chimera state for $N = 100$. (d) Phase diagram for $N = 100$ oscillators. Other parameters as in Fig. 2.

[1] M. J. Panaggio and D. M. Abrams, Nonlinearity **28**, R67 (2015).
[2] Y. Kuramoto and D. Battogtokh, Nonlinear Phenom. Complex Syst. **5**, 380 (2002).
[3] D. M. Abrams and S. H. Strogatz, Phys. Rev. Lett. **93**, 174102 (2004).
[4] G. C. Sethia, A. Sen, and G. L. Johnston, Phys. Rev. E **88**, 042917 (2013).
[5] A. Zakharova, M. Kapeller, and E. Schöll, Phy. Rev. Lett. **112**, 154101 (2014).
[6] C. R. Laing, Phys. Rev. E **92**, 050904(R) (2015).
[7] B. K. Bera and D. Ghosh, Phys. Rev. E **93**, 052223 (2016).
[8] B. K. Bera, D. Ghosh, and M. Lakshmanan, Phys. Rev. E **93**, 012205 (2016).
[9] A. M. Hagerstrom, T. E. Murphy, R. Roy, P. Hövel, I. Omelchenko, and E. Schöll, Nat. Phys. **8**, 658 (2012).
[10] M. R. Tinsley, S. Nkomo, and K. Showalter, Nat. Phys. **8**, 662 (2012).
[11] E. A. Martens, S. Thutupalli, A. Fourriere, and O. Hallatschek, Proc. Natl. Acad. Sci. (USA) **110**, 10563 (2013).
[12] L. Larger, B. Penkovsky, and Y. Maistrenko, Nat. Commun. **6**, 7752 (2015).
[13] J. D. Hart, K. Bansal, T. E. Murphy, and R. Roy, Chaos **26**, 094801 (2016).
[14] N. Lazarides, G. Neofotistos, and G. P. Tsironis, Phys. Rev. B **91**, 054303 (2015).
[15] J. Hizanidis, N. Lazarides, G. Neofotistos, and G. P. Tsironis, arXiv:1601.04843v1 [nlin.CD].
[16] P. S. Dutta and T. Banerjee, Phys. Rev. E **92**, 042919 (2015).
[17] J. Hizanidis, E. Panagakou, I. Omelchenko, E. Schöll, P. Hövel, and A. Provata, Phys. Rev. E **92**, 012915 (2015).
[18] V. M. Bastidas, I. Omelchenko, A. Zakharova, E. Schöll, and T. Brandes, Phys. Rev. E **92**, 062924 (2015).
[19] N. C. Rattenborg, C. J. Amlaner, and S. L. Lima, Neurosci. Biobehav. Rev. **24**, 817 (2000).
[20] N. C. Rattenborg, Naturwissenschaften **93**, 413 (2006).
[21] J. Hizanidis, N. E. Kouvaris, G. Zamora-López, A. Díaz-Guilera, and C. G. Antonopoulos, Sci. Rep. **6**, 19845 (2016).
[22] I. Omelchenko, O. E. Omelchenko, P. Hövel, and E. Schöll, Phys. Rev. Lett. **110**, 224101 (2013).
[23] N. Semenova, A. Zakharova, V. Anishchenko, and E. Schöll, Phys. Rev. Lett. **117**, 014102 (2016).
[24] A. Vüllings, J. Hizanidis, I. Omelchenko, and P. Hövel, New J. Phys. **16**, 123039 (2014).
[25] J. Hizanidis, V. Kanas, A. Bezerianos, and T. Bountis, Int. J. Bifurcation Chaos **24**, 1450030 (2014).
[26] E. Izhikevich, *Dynamical Systems in Neuroscience: The Geometry of Excitability and Bursting* (MIT Press, Cambridge, MA, 2007).
[27] I. Belykh, R. Reimbayev, and K. Zhao, Phys. Rev. E **91**, 062919 (2015).
[28] W. Zou, C. Yao, and M. Zhan, Phys. Rev. E **82**, 056203 (2010).
[29] M. Zhan, J. H. Gao, Y. Wu, and J. H. Xiao, Phys. Rev. E **76**, 036203 (2007).
[30] J. Xiao, G. Hu, J. Yang, and J. Gao, Phys. Rev. Lett. **81**, 5552 (1998).

[31] I. Aranson, H. Levine, and L. Tsimring, Phys. Rev. Lett. **72**, 2561 (1994).
[32] J. L. Hindmarsh and M. Rose, Proc. R. Soc. London, Ser. B **221**, 87 (1984).
[33] B. Igor and M. Hasler, Patterns of Synchrony in Neuronal Networks: The Role of Synaptic Inputs, in *Nonlinear Dynamics: New Directions* (Springer International Publishing Switzerland, 2015).
[34] I. Belykh, E. de Lange, and M. Hasler, Phys. Rev. Lett. **94**, 188101 (2005).
[35] T. Kapitaniak, P. Kuzma, J. Wojewoda, K. Czolczynski, and Y. Maistrenko, Sci. Rep. **4**, 6379 (2014).
[36] P. Jaros, Y. Maistrenko, and T. Kapitaniak, Phys. Rev. E **91**, 022907 (2015).
[37] I. Omelchenko, A. Provata, J. Hizanidis, E. Schöll, and P. Hövel, Phys. Rev. E **91**, 022917 (2015).
[38] M. Wolfrum and O. E. Omelćhenko, Phys. Rev. E **84**, 015201(R) (2011).
[39] A. Prasad, M. Dhamala, B. M. Adhikari, and R. Ramaswamy, Phys. Rev. E **81**, 027201 (2010).
[40] I. Berenstein and Y. De Decker, J. Chem. Phys. **143**, 064105 (2015).
[41] F. P. Kemeth, S. W. Haugland, L. Schmidt, I. G. Kevrekidis, and K. Krischer, arXiv:1603.01110 [nlin.CD] (2016).
[42] B.-W. Li and H. Dierckx, Phys. Rev. E **93**, 020202(R) (2016).
[43] S. I. Shima and Y. Kuramoto, Phys. Rev. E **69**, 036213 (2004).